Molecular motor organization and mobility on cargos can overcome a tradeoff between fast binding and run length

Matthew Bovyn[1,5], Steven Gross[2,1,3,5], Jun Allard[1,4,5*],

1 Department of Physics and Astronomy, University of California, Irvine, Irvine, California, USA
2 Department of Developmental and Cell Biology, University of California, Irvine, Irvine, California, USA
3 Department of Biomedical Engineering, University of California, Irvine, Irvine, California, USA
4 Department of Mathematics, University of California, Irvine, Irvine, California, USA
5 Center for Complex Biological Systems, University of California, Irvine, Irvine, California, USA

* jun.allard@uci.edu

Abstract

Cellular cargos, including lipid droplets and mitochondria, are transported along microtubules using molecular motors such as kinesins. In the cell, it is unclear how motors are coordinated to achieve transport outcomes that are cargo-specific. One possibility is that transport is modulated by differences in organization and mobility of motors on the cargo's surface. We use mechanochemical 3D computational modeling to compare different motor anchoring modes, and find that organizational changes can optimize for different objectives. Cargos with clustered motors are transported efficiently, but are slow to bind to microtubules. Cargos with motors dispersed rigidly on their surface bind microtubules quickly, but are transported inefficiently. Cargos with freely-diffusing motors have both fast binding and efficient transport, although less efficient than clustered motors. These results point to a functional role for observed changes in motor organization on cargos, and suggest motor diffusivity as a control point for transport, either by modulation of adaptor proteins or changes in lipid composition.

Author summary

The molecular motors of the kinesin family are responsible for moving the parts of cells to their subcellular destinations, organizing the cell interior. Computational modeling has historically played an important role in understanding how these motors work. But, strikingly, most models assume the subcellular cargos have rigid surfaces. Simulating fluid surfaces is more challenging but more applicable to biological cargo. In this work, we build a computational model of molecular motor transport of cargo with fluid surfaces. Surface fluidity gives cargo transport new properties, like enhanced transport efficiency, and the ability to push against opposing forces. Because the effects of surface fluidity vary strongly with some of the properties of the cargo, like its size, our results hint at one of the ways that the same transport machinery can distinguish different cargo despite using the same motors.

Introduction

To organize their internal structure, eukaryotic cells employ molecular motors in the kinesin and dynein superfamilies to transport organelles and other cargo along microtubules. Despite having only a limited set of cargo transport motors (kinesin-1, kinesin-2 and kinesin-3 families [1], along with cytoplasmic dynein), different cargos are transported to different locations, even though they are transported along the same set of microtubule "roads". For example, under normal conditions COS-7 cells direct lipid droplets toward microtubule plus end, localizing them near the plasma membrane, and mitochondria toward the minus end, localizing them near the nucleus. Under glucose starvation, localization of both organelles changes to spread them out around the cell, allowing them to come into contact with each other [2]. How do cells achieve these cargo-specific routing outcomes? In some cases, cells use molecular specificity to achieve cargo specificity, such as using specific linkers or cargo-bound regulators [3, 4].

However, recent experiments suggest cells may use other methods as well. Transport may be regulated in ways that are not based on biochemical specificity, but rather, utilize physical properties of the cargo. For example, routing could be affected by cargo size, and where and how motors are attached to the surface of the cargo. In J774 macrophages, larger phagosomes are transported directly toward the nucleus while smaller ones spend more time moving bi-directionally [8]. In *Dictyostelium*, dynein organization on the cargo surface changes from spread out to clustered as phagosomes mature [9]. Past work using computational modeling has called attention to motor organization as a regulator of transport [10].

Many cellular cargos are encased in membranes, raising the possibility that motors diffuse in that membrane. Freedom of motors on the surface of cargos has been of recent experimental interest and several papers have compared the collective action of kinesin motors which are free to diffuse in membranes to cases where they are rigidly attached to a surface, both in the microtubule gliding assay configuration [11] and the bead assay configuration [12]. These studies show that motor freedom in membranes can influence transport properties, but it is unclear how to translate the *in vitro* results into the context of the cell, especially since transport is slowed in the gliding assay, while it is sped up in the bead assay. Furthermore, Li et al. find that the increase in velocity is small with no difference in how far cargos travel overall. This confounds the impact which freedom to diffuse may have on cargo transport in the cell.

One key challenge that has been overlooked so far is the time required to initiate transport; that is, for the cargo to diffuse over to the microtubule, and subsequently for the motors to bind, initiating transport. In the cell, with significantly higher viscosity than in vitro, this initiation step may be much more challenging. To gain intuition for how the above experiments, which were performed *in vitro*, may be extrapolated into the cellular environment, we perform a simple calculation. We ask how long it would take for a motor initially located opposite the microtubule to come within range of the microtubule to bind to it, under two different assumptions of how that motor is able to move: first by rotational diffusion of the cargo body moving a rigidly bound motor, and second by diffusion of a motor in the membrane of a non-moving cargo (illustrated in the diagrams accompanying Fig 1 A and B respectively). By examining Fig 1, we find that for any choice of cargo size, the time it takes for a motor to come near enough to the microtubule to bind is similar for cargo rotational diffusion at the viscosity of water ($\sim 0.001\,\mathrm{Pa\,s}$) and for surface diffusion at the diffusion coefficient of motors in the *in vitro* supported lipid bilayers used in the experiments mentioned above ($\sim 1\,\mu\mathrm{m}^2\,\mathrm{s}^{-1}$). For the cargos used in bead assays (less than $1\,\mu\mathrm{m}$ diameter), both these modes have times which fall in the range of characteristic times proposed for motor binding [13–15]. However, cargos in the cell have been repeatedly measured to diffuse less freely than in water. While a wide range of viscosity values has been inferred from these

Fig 1. Mean first passage times (MFPTs) for a motor initially located opposite the microtubule to come within binding range by:
A: rotational diffusion of the cargo. Shown for various values of viscosity of the surrounding fluid. Values are chosen to span the range of values estimated for cytoplasm [5]. Grey curve is at viscosity 0.4 Pa s, measured in [6].
B: diffusion of the motor in the cargo surface. Shown at various values of the diffusion coefficient. MFPTs for diffusion coefficients achievable when the surrounding fluid has viscosity of 0.4 Pa s are shaded in grey [7].
For details on calculation, see S1 Fig.

measurements [5], the most similar measurement we know of to the specific case of a $\sim$ 1 µm cargo rotating was made by Wilhelm and colleagues [6]. They find a viscosity of 0.4 Pa s, several hundred times greater than water (Fig 1A, thick grey line) and similar to the viscosity used in [16]. For more details on this choice of viscosity, see S1 Appendix section 2.1.3. At this viscosity, rotational diffusion times are several orders of magnitude slower than in water. Importantly, they are also several orders of magnitude slower than diffusion of motors at typical values of diffusion coefficients for cellular transmembrane proteins (Fig 1B, thick line, BioNumbers BNID:114189 [17]). For more details on this calculation, see S1 Fig.

The drastic differences in the time it takes for a motor to enter binding range of the microtubule between rotational diffusion of the cargo and the translational diffusion of a motor in the cargo membrane evoke the possibility that the time for a cargo to bind to a nearby microtubule in the cell could be drastically changed by the freedom of motors to diffuse. The subsequent transport of a cargo also depends strongly on the number of motors that are able to access the microtubule [10]. Therefore, motor freedom also has the potential to change other important transport properties such as run length and force generation.

The calculation plotted in Fig 1 is highly simplified: it ignores binding times, motor on rates, and does not tell us about subsequent transport. Furthermore, cellular cargos are often moved by several motors simultaneously [18]. In this paper, we seek a comprehensive look at how cargos with different motor organizations are transported, with a focus on the less-explored case of cargos which have motors that are free to diffuse in the membrane. This requires us to compare transport properties over a wide range of membrane fluidities, from fluid to solid. We construct a computational model of cargo transport which includes multiple motors which are able to diffuse in the cargo membrane. While there is a rich history of theoretical studies of motor-based transport [19, 20], the ability to describe the full range of membrane fluidity represents a significant advance. Since there are two viscosities in the system (the membrane and the cytoplasm), forces translate into motion in a non-trivial, coupled manner that must be re-calculated at every simulation timestep. Furthermore, the two viscosities induce diffusion (thermal fluctuations) with different amplitudes, so motors experience statistically correlated noise. (Several recent models have included motors that rearrange on the cargo [16, 21]; however, they limited their studies to parameter regimes in which the complicating factors above were absent.) The results of our computational model reveal that the changes in motor organization and mobility have significant impact on microtubule binding, transport and force generation.

Fig 2. Motor organization modes and simulation snapshots.
A: Motors anchoring modes to be investigated. Cargo shown in yellow, motors in blue and microtubule in green. We name the states: rigid clustered (**i**), rigid dispersed (**ii**), free independent (**iii**), and free clustered (**iv**).
B: Series of simulation snapshots. The cargo is in yellow and the microtubule in green. The blue hemispheres represent the reach length of unbound motors, which have their anchor point at the center of the hemisphere. Bound motors are represented with a magenta stalk, small black anchor point and larger blue sphere at the center of mass location of the motor heads.

Results

A computational model of cargo transport including freedom of motors to diffuse in the cargo membrane

We wish to explore the impact of different classes of surface organization of motors on specific transport outcomes. Because there are an infinite number of ways to arrange motors on a cargo, we narrow our scope to a few specific cases. We choose four extreme cases, as shown in Fig 2A, which we term organization modes. The first two modes have motors bound rigidly to the cargo. They differ in how motors are spaced; the first mode we term "rigid clustered" places all the motor anchors at the same point, while in the second mode, which we term "rigid dispersed", the motor locations are random, drawn from a uniform distribution over the surface. The other two modes have motors which are free to diffuse in the cargo surface. In the "free independent" mode, the motor anchors do not interact with each other, other than through forces they exert on the cargo. In the final mode, termed "free clustered", all motor anchors are bound together, but the ensemble is able to diffuse in the cargo membrane. In this mode, we assume the cluster of motors diffuses with a reduced diffusion coefficient so that $D \sim 1/\sqrt{N}$ where N is the number of motors, which is consistent with motors being arranged in roughly a disk [7] (rather than, e.g., in a row).

To investigate transport outcomes of cargos in these four different organization modes, we construct a three dimensional model of a cargo, the motors, and a microtubule. We model the cargo as an undeformable sphere. We attach motors to the cargo at points which we term the anchors. We model these motors using the well studied chemomechanics of kinesin-1. These motors can bind the microtubule when the anchor is within reach of the microtubule (blue hemispheres in Fig 2B represent motor reach length). Once bound, they step along the microtubule and unbind from it with rates that have been intensely studies *in vitro*. We draw our chemomechnical model for kinesin from recent experimental [23] and modeling [24] efforts. For more details, see S1 Appendix sections 1.1.1 and 1.3.

As motors step, they exert forces on the cargo which would both tend to pull the cargo along through the surrounding fluid, and drag the anchor through the cargo membrane. In our model, forces which would drag the anchor through the cargo membrane result both in displacement of the anchor in the membrane and rotation of the cargo, in proportion to the anchor diffusion coefficient. Forces acting to move the cargo body do so against viscous drag, as we model the surrounding fluid as Newtonian. While recent measurements suggest the cytoplasm is an actively-driven, complex fluid with significant elasticity [25, 26], methods for simulating diffusion and the effect of further active forces in this environment are still in development. Modeling the cytoplasm surrounding the cargo as Newtonian allows us to qualitatively capture that some cargos in cells may be relatively free to move, while others may be significantly impeded by their local environment. For more information, see S1 Appendix.

Both cargo and motors diffuse in their respective (3D or 2D) fluids. The cargo diffuses both rotationally and translationally with statistics governed by the Fluctuation-Dissipation Theorem, as implied by the viscosity of the surrounding fluid. Motors diffuse in the cargo surface with statistics governed by a diffusion coefficient. In general, complex movement may result from the interaction of motor anchors with different lipid domains [9] or other structures (for example, diffusion of cell surface proteins is influenced by the underlying actin cortex [27]).

A full description of the model and derivation of the equations we simulate can be found in S1 Appendix section 1. The simulation framework is detailed in S1 Appendix section 2 and parameter values listed in table A1 are used for all simulations, unless otherwise indicated.

To obtain transport properties of cargos in different organization modes, we simulate 100 or more stochastic trajectories and examine the resulting distributions. We simulate trajectories using a hybrid Euler-Maruyama-Gillespie scheme, and report a series of tests which show that the code reproduces expected results in some simplified situations in supplemental section S1 Appendix section 3. Snapshots from a single trajectory are shown in Fig 2B. As time progresses, motors diffuse around the surface of the cargo, motors bind and unbind from the microtubule, and cargo orientation changes as it is pulled along by forces generated by the motors, as shown in S1 Video.

Cargos with free motors bind to the microtubule faster than those with rigidly anchored motors

For a cargo to be transported, one of its motors must first bind the microtubule. In this section, we use our model to investigate the time it takes for a cargo located near a microtubule to bind to it. Visualizations of example simulations for each organization mode are shown in S2 Video–S5 Video.

We first compare the four organization modes as a function of the number of motors on the cargo, as Fig 3A shows for a 0.5 µm diameter cargo. We find that for cargos in the rigid clustered mode, the mean time to bind is long when there is a single motor, and stays constant as the number of motors on the cargo increases. This can be understood by considering the timescales in the problem; cargos in this mode spend most of their time waiting until the motors are near enough to the microtubule for them to bind, as rotation is slow compared to the characteristic binding time of a single motor. A cargo in the rigid dispersed mode with only one motor is identical to a rigid clustered cargo with one motor. For rigid dispersed cargos, however, we find the time to bind decreases drastically as more motors are added. Because anchor locations are selected randomly from a uniform distribution over the surface of the cargo, the average angle though which these cargos must rotate before a motor comes within reach of the microtubule decreases as motors are added. This change is most drastic for the first few motors, with the time to bind of these 0.5 µm diameter cargos decreasing by an order of magnitude with the addition of only 5 motors.

We find that 0.5 µm diameter cargos with a single free motor with diffusion coefficient $0.1\,\mu m^2\,s^{-1}$ bind more than an order of magnitude faster than cargos of the same size with a single rigidly attached motor. This also can be understood by considering timescales: diffusion on the surface is much faster than rotational diffusion of the cargo, so less time is spent waiting for a motor to come near the microtubule. When free motors are added in a cluster, we find that time to bind is independent of the number of motors in that cluster. This indicates that the time spent waiting for motors to come near the microtubule is the slowest process, as the increased binding rate of the motors in the cluster do not decrease the time to bind. When anchors are independent, time to bind goes down drastically as the number of motors is increased. This effect

Fig 3. Times for cargos in different organization modes to bind to the microtubule Simulated cargos are allowed to diffuse rotationally, but not translationally, with no gap between the cargo and microtubule. In all panels, error bars represent standard error of the mean of 300 simulations. Underlying distributions are approximately exponential (see S2 Fig).
A: Time for the cargo to bind to the microtubule for the four anchoring modes, as a function of the number of motors on the cargo. The characteristic time for a single motor to bind, assuming it is near the microtubule, is shown in dashed grey. Distributions of times to bind in the different modes are shown in S2 Fig, A. Overlaid curves are fits, detailed in S1 Table.
B: Dependance of the cargo binding time on the diffusion coefficient of the motor anchors in the cargo membrane for the free independent mode. Red errorbars located on the left vertical axis are mean binding time for the rigid dispersed mode, to which the free independent mode reduces at low diffusion coefficients. Distributions of binding times at the indicated diffusion coefficients are shown in S2 Fig, Bi. Distributions of binding times for the lowest diffusion coefficient and rigid dispersed cargos are shown together in S2 Fig, Bii. Lines between points are guides for the eye.
C: Time for the cargo to bind as a function of the cargo radius for the four anchoring modes (**i-iv**), shown for various values of the number of motors on the cargo, N. Dashed lines indicating scaling with diameter to the fourth power (i and ii) and diameter to the second power (iii-iv) are shown for comparison. Overlaid curves are fits, detailed in S1 Table.

includes both the decreased time to bind from the spread out initial locations of the motors, as well as the fact that each motor performs its own search. While anchor motions are all subject to the same contribution from the rotational diffusion of the cargo, the rotation timescale is much slower than surface diffusion, making each search almost independent at this cargo size and diffusion coefficient.

The results of Fig 3A indicate that at $0.1\,\mu\text{m}^2\,\text{s}^{-1}$, surface diffusion is much faster than cargo rotation. At some diffusion coefficient, surface diffusion should become slower than cargo rotation, and the time to bind for free independent cargos should approach that of rigid dispersed cargos. We find that the motor diffusion coefficient must be decreased by orders of magnitude to obtain significant changes in the time to bind, as shown in Fig 3B. For the $0.5\,\mu\text{m}$ diameter cargos shown, diffusion coefficient of the motors must be lower than $10^{-4}\,\mu\text{m}^2\,\text{s}^{-1}$ for free independent cargos to have times to bind similar to rigid dispersed cargos.

We find that times to bind for cargos in each of the organization modes depend differently on the cargo size. When cargos are small enough that all motors can simultaneously reach the microtubule ($\sim$50 nm diameter), the time to bind for cargos in all organization modes is the same. As cargo size increases, time to bind remains dependent only on motor number until cargos reach $\sim$100 nm in diameter. For cargos larger than this, scaling of time to bind with size is drastically different for cargos in the different organization modes. For cargos with rigidly attached motors, time to bind scales with approximately the fourth power of the cargo diameter. For cargos in the free independent mode, time to bind scales with only (roughly) the second power of the diameter. Free clustered cargos with one motor are identical to free independent cargos with one motor, and therefore must have the same scaling. As the number of motors increases, however, scaling becomes more severe, nearing the scaling of rigid motors at high motor number.

Fig 4. Free independent cargos have longer run lengths than rigid dispersed cargos due to dynamic clustering
A: Position (top) and number of motors engaged (bottom) with time for free independent cargos with 12 total motors. Trajectories of three cargos are shown in black and the mean over 100 cargos is shown in dark blue. Cargos are excluded from the calculation after they fall off the microtubule. The area between the 5th and 95th percentile positions is shaded in blue in the top panel. Times greater than the time to steady state are shaded in grey in the bottom panel.
B: Mean run lengths for cargos in each of the three anchor modes as a function of the total number of motors on the cargo. Distributions of run lengths are shown in S3 Fig, A.
C: Mean number of motors engaged at steady state versus motor number for the 3 anchor modes. Linear fits are shown as dotted lines. For values, see S1 Table. Grey box indicates conditions with similar mean number engaged at steady state which will be compared in later figures.
D: Mean run length as a function of steady state number of engaged motors for the three anchoring modes.
E: Mean run length for cargos with three total motors as a function of cargo size for each of the three anchoring modes.
F: Mean run length for cargos with free independent motors as a function of the diffusion coefficient of the motors in the cargo membrane, for different numbers of total motors. Red errorbars overlaid on the left axis are for rigid dispersed cargos of the same total numbers.
In B, E and F, error bars are SEM of 300 cargos. In C, error bars are SEM of 100 cargos. In B, D, E and F lines between points are guides for the eye.

Cargos with free independent motors form dynamic clusters which increase travel distance

We next investigate the distance that cargos travel, after initial attachment to the microtubule. To do so, we begin simulations with a single motor bound to the microtubule and simulate until the cargo reaches a state in which all motors are detached from the microtubule. A few stochastic trajectories, along with the mean position over many cargos are shown as a function of time in Fig 4A (top). Once bound to the microtubule, rigid clustered cargos and free clustered cargos behave similarly. Hereafter, we show only results for rigid clustered cargos and refer to them as "clustered" to reflect this. Visualizations of example simulations for each organization mode are shown in videos S6 Video–S8 Video.

We find that cargo run lengths depend strongly on motor organization mode. For cargos with clustered motors, just four motors working together give run lengths on the order of the size of a cell. Motors in this mode work together very well, as if any motor is bound the rest of the motors are located where they are also able to bind the microtubule. This contrasts with the dispersed mode, where many motors are necessary to achieve run lengths of a few microns. For the 0.5 µm diameter cargos plotted in Fig 4B, 25 motors are required to achieve a mean run length of 3 µm. These results are consistent with previous work comparing these two modes [10].

For cargos with free independent motors, we find run lengths which are longer than those of dispersed cargos, but not as long as those of clustered cargos. One possibility is that the run lengths are due to the number of motors which are instantaneously bound to the microtubule at a given time, which we term the number engaged. We therefore query this quantity in our simulations. The number of motors engaged on the microtubule fluctuates with time. Several stochastic trajectories are shown in Fig 4A

(bottom), along with the mean over 100 cargos at each time. We find that the mean number of motors engaged rises from the initial condition of 1 to a steady state value over a period of time. In Fig 4C, we show that free independent cargos have more motors engaged than rigid dispersed cargos. The initial locations of motors on the surface of cargos in these two modes is the same, i.e., uniformly random on the surface. Therefore, the increased steady state number of engaged motors on free independent cargos indicates that motors are diffusing to the microtubule, binding, and remaining bound for longer than they would if simply placed randomly. In other words, the motors cluster near the microtubule. These clusters are dynamic, with motors diffusing in and binding, as well as unbinding and diffusing away, as can be seen in S1 Video and S8 Video.

How strong is the clustering effect? In the range of total motor numbers investigated, the number of engaged motors is 25 % to 30 % of the total number on the cargo. This is more than the 10 % to 15 % of motors engaged on rigid dispersed cargos, but less than the $\sim 80\,\%$ of motors engaged on clustered cargos (Fig 4C). So, while dynamic clusters contain more motors than would available to bind the microtubule if motors were distributed randomly on the surface, they do not contain all or even most of the motors on the cargo.

We hypothesized that dynamic clustering is responsible for free independent cargos' enhanced run length over rigid dispersed cargos. To test this hypothesis, we plot mean run length vs. steady state number engaged. If dynamic clustering is responsible for the enhanced run length, we expect the free independent and rigid clustered modes to have the same run length when the number of engaged motors is the same. We see in Fig 4D that data from the two modes is similar. Run lengths for free independent cargos are in fact slightly lower once corrected for number of engaged motors. This is surprising because cargos with similar mean numbers of motors engaged at steady state have similar distributions of motors engaged, as shown in S3 Fig, B. In supplementary S3 Fig, C, we show that the lower run length is explained by a longer time to steady state and resultantly more cargos which fall off the microtubule at early times.

The three modes also differ significantly in their dependance on cargo size. In Fig 4E, we show that cargos with clustered motors have a run length that depends only weakly on cargo size, while free independent and rigid dispersed cargos have a more complex dependance.

The run length advantage of free independent cargos over rigid dispersed ones should, like the binding time advantage, be reduced to zero at low anchor diffusion coefficients. In Fig 4F, we show that the diffusion coefficient must be reduced by orders of magnitude to have significant impacts on run length. We find that diffusion coefficients below $10^{-4}\,\mu m^2\,s^{-1}$ are effectively rigid, which is a similar to the threshold we found for time-to-bind.

Cargos with free independent motors are better able to transport against a load compared to cargos with rigid dispersed motors

A cargo's ability to generate a sustained force is also important for navigating the crowded environment of the cell. In this section, we examine the run lengths of cargos in the different organization modes against a constant force.

As expected, we find that that increasing force decreases the run length of cargos, no matter what the organization mode or number of motors, as can be seen in S4 Fig, A. We find that 7 pN of force is sufficient to reduce the run lengths from 20 µm or more to nearly zero in every organization mode.

We now compare the run length of cargos in different organization modes under

Fig 5. Cargos with free independent motors travel farther under load due to dynamic clustering.
Mean run lengths as a function of external hindering load on the cargo for cargos in each of the three modes, with
A: matched total number of motors. Cargos with 20 clustered motors travel farther than 20 µm on average, and are not shown to clarify the difference between rigid dispersed and free independent modes.
B: matched number of motors engaged at steady state (at 0 external load). Distributions of run lengths for these cargos can be found in S4 Fig, C.
Error bars are standard error of the mean over 300 cargos in both A and B. Lines between points are guides for the eye.

force. In Fig 5A, we show that cargos with 20 free independent motors have significantly longer run lengths than cargos with the same number of rigid dispersed motors, when subject to forces up to 7 pN. At higher forces, run lengths for these cargos are effectively zero. At this high number of motors, cargos with clustered motors travel long distances, even when loaded with 12 pN or more (Fig 5A, arrows). When the number of total motors is 5, we can see that cargos with clustered motors outperform both rigid dispersed and free independent cargos (S4 Fig, B). At this low number of total motors, cargos in rigid dispersed and free independent modes are almost always driven by a single motor, so differences between the two modes are not apparent.

Is the increase in run lengths under force also solely due to changes in the number engaged? To test this hypothesis, we plot run lengths under force for cargos in the three organization modes with total numbers of motors which give the cargos matching steady state numbers of engaged motors (at 0 force, indicated by box in Fig 4C). Like in the zero force case, when we compare at the same steady state number, we find that cargos with free independent motors have similar, but slightly lower run lengths than cargos with dispersed motors. Therefore, the enhancement in run length of free independent motors comes from the ability of motors to form dynamic clusters, like in the unloaded case.

A priori, we hypothesized that free motors share the load more equally, and that this would lead to longer run lengths under load, after correcting for number engaged. However, we do not find this effect is strong enough to outperform cargos with rigid dispersed motors on a per-motor-engaged basis.

Discussion

While transport of subcellular cargo by molecular motors is increasingly understood, the extension of this understanding to control of cell internal organization will involve studying the three-way interplay between the cargo, the MT and local environment, and the motors. In this work, we developed a computational model of the motors' interaction with the cargo, assuming different modes of organization. These modes varied both in the positions of the motors on the surface of the cargo and the freedom of those positions to change via movement in a fluid membrane. We found that cargos with rigidly attached motors face a tradeoff between, on the one hand, time for the cargo to bind to a nearby microtubule and, on the other, the run length of cargos once one motor is bound. Rigid clustered motors bind slowly, but have long run lengths. Rigid dispersed cargos bind faster than rigid clustered cargos, but have short run lengths. Our main result is that, depending on parameters, cargos with free motors can overcome this tradeoff (Fig 6). Cargos with free independent motors bind faster than cargos in either of the rigid modes, and have run lengths which are longer than those of

Fig 6. We find that different organizations of the motors on the cargo have different implications for how rapidly the cargo will bind to a nearby microtubule and the cargo's ability to travel along the microtubule. For cargos with motors rigidly bound, (first two columns) there is a tradeoff between clustered motors, which are slow to bind the microtubule, but travel long distances, and dispersed motors, which bind the microtubule quickly but are have poor travel distances. Cargos with freely diffusing motors (third column), at reasonable surface diffusion coefficients, cargo sizes and motor numbers, overcome this tradeoff. They bind the microtubule at least as fast as rigidly dispersed motors, and faster for large and realistic estimates of diffusion coefficient. They travel farther than rigid dispersed motors because of the formation of dynamic clusters. Because these clusters have high internal turnover, travel distances are lower than that of a rigid cluster. For a cargo with a freely diffusing cluster of motors (fourth column), cargo binding may behave more like a rigid cluster or freely diffusing motors, depending on parameters. Once it has bound the microtubule, it behaves indistinguishably from a rigid cluster in both run length and force generation.

rigid dispersed cargos, but not as long as clustered cargos. When motors are arranged in a free cluster, cargos have the same long run lengths as rigid clusters, as well as binding to a nearby microtubule more quickly. The time to bind is not as fast as a free independent cargo, however, or even a rigid dispersed cargo with many motors.

This work adds to a growing body of evidence that, first, the position of motors on the cargo (whether free or not) impacts transport [10, 28]; second, that mobility on the cargo surface further influences transport [11, 12, 16, 21, 29]; and, third, that there are significant differences in the arrangement of motors on cargo in cells [9, 16], for example via changes to lipid content [30, 31]. The closest direct experimental study related to our work is by the Xu Lab [12]. That work was done in vitro, where the cargo is immersed in a fluid with a viscosity orders of magnitude smaller than the one used in this paper. They find broad agreement with our simulations that fluid membranes enhance transport. However, the details are different: The velocity changes are weak and run-lengths changes are undetectable. Our work thus highlights an important role for the rheological properties of the cytoplasm, and the difficulty extrapolating in vitro results into the cellular environment.

We find that time to bind and run length are sensitive to cargo size in different ways for the four organization modes. Rigid clustered cargos have a time to bind which scales up strongly as cargo size increases, but run length is relatively insensitive to cargo size. The time to bind for rigid dispersed cargos also scales strongly, but their run length is more sensitive to cargo size in comparison to rigid clustered cargos. Free independent cargos have a much weaker scaling of time to bind, as well as an intermediate dependance of run length on cargo size. These different scalings raise the possibility that the cell could use the size dependent behaviors to differentially direct otherwise similar cargos.

Moreover, the differences in scaling law exponents we uncover are independent of model details, e.g., motor parameters and molecular numbers. Therefore, binding time scaling could be used to identify the organization of motors on cargos from the cell. Using the natural variability of cargo sizes to uncover different scaling exponents could inform whether the motors are free or not.

Our work is in broad agreement with Chowdary et al. [16], who combined advanced microscopy and tracking with a computational model to give insight into the motion of endosomes in axons. They report the emergence of dynamic clustering in their simulation via preference for binding the MT track. Their simulation allows motors to move on the surface of a cargo independent of each other and of rotations of the cargo itself. Our work extends this by considering a model in which motor anchor position,

cargo rotation and cargo translation are all coupled with both cytoplasmic viscosity/fluctuations and membrane viscosity/fluctuations, via a force-balance relationship at every time point. Particularly interesting complexity arises, e.g., the two viscosities give rise to fluctuations that are, in the lab frame of reference, no longer uncorrelated (see S1 Appendix). Doing so allowed us to explore a wide range of parameters, from the limit in which the cargo membrane is nearly inviscid and the motor can step along the MT without significantly moving the cargo, all the way to a static anchoring. It also allowed us to explore the competition between cargo rotation and diffusion of motors to drive binding time – of particular importance when the cargos are small. The coupling via force-balance also led to an emergent inter-motor communication via how each motor is loaded, which influenced predicted run lengths. Interestingly, we find that dynamic clustering is not a strong effect for all parameters regimes. For example, at reasonable parameters, we find only 25% of the motors are clustered (e.g., Fig 4).

Many cargo in cells are stopped or spend significant fraction of time not moving, including lipid droplets [32] and mitochondria [33]. There are several possibilities to explain this: a regulatory state where transport is deactivated; a tug-of-war between motors of different directionalities (possibly of the same species [34]); or an absence of motors on this cargo. However, our results suggest another possibility: We find for cargo with rigid clustered motors, especially large ones, the time to bind a nearby microtubule is extremely large, on the order of tens of minutes.

That the transport machinery is sensitive to motor organization opens several possible directions of future work. First, cargos in the cell exist in a microtubule network with a specific architecture [15, 35–37]. The current work focused on exploring interaction with a single MT, but could readily be extended. Second, many cargos are deformable [38] and this might lead to significant differences in transport. While deformability of a large cargo will lead to transport changed by interacting with the environment, e.g., spacing of nearby cytoskeletal elements and organelles, our work suggests cargo deformability might also impact transport more directly via changes to motor organization. Finally, motors are sensitive to MT-associated proteins (MAPs) [39, 40]. The accessibility of the motors to MAPs is expected to exhibit similar behavior to the accessibility of motors to the MT, which we have shown varies widely depending on organization mode.

Supporting information

S1 Fig. Mean reach elevation and calculation of mean first passage time to the microtubule. In figure 1 we show an estimate of the time it would take for a motor, initially opposite the microtubule, to come within reach of it. These times come from analytical expressions for mean first passage time to a spherical cap, $\frac{8\pi\eta R^3}{k_B T}\log\left(\frac{1-\cos(\pi)}{1-\cos(\theta)}\right)$ for rotational diffusion of the cargo and $\frac{R^2}{D}\log\left(\frac{1-\cos(\pi)}{1-\cos(\theta)}\right)$ for diffusion in the cargo surface [41]. Here η represents viscosity (of the fluid surrounding the cargo), R is the cargo radius, k_B is Boltzmann's constant, T is temperature, and D is diffusion coefficient (of the motor in the cargo surface). To apply these equations, we had to first estimate θ, the extent of the spherical cap to which the motor must diffuse before binding. To do so, we simulated motors diffusing from the north pole of the cargo and recorded the first anchor location where the motor was able to bind with its maximum rate as described in S1 Appendix section 1.3.3, referred to as a max reach location. We then used the mean elevation of these points as our estimate for θ. Cargo and microtubule were situated as shown in A. For details on how we model the mechanics of a motor and it's attachment to the cargo, see S1 Appendix section 1.1.1.

A: Mean reach elevation for cargos of various sizes, as labeled in each panel. Legend in final panel applies to every other panel.

B: Mean reach elevation for each cargo size shown in A. Bars represent standard error of the mean. Data are well fit to reach elevation $\theta = (.27/d)^{.7}$, where d is cargo diameter (black curve).

S2 Fig. Distributions of times for cargos to bind to the microtubule.

Ai-iv: Empirical cumulative distributions of time to bind for cargos in each of the four organization modes. Thinner curves of the same color are exponential fits to the data.

Bi: Empirical cumulative distributions for free independent cargos with a range of motor diffusion coefficients D. Diffusion coefficients are log spaced, values of D for each distribution shown are labeled on the colorbar. Thinner curves of the same color are exponential fits to the data.

Bii: Empirical cumulative distributions of times to bind for free independent cargos at diffusion coefficient $D = 1 \times 10^{-5}\,\mu\text{m}^2\,\text{s}^{-1}$ for several numbers of motors on the cargo (yellows). Also shown are distributions for rigid dispersed cargos at the same numbers of total motors (reds). Thinner curves of the same color are exponential fits to the data. Dashed curves are fits for rigid dispersed cargos.

S3 Fig. Distributions of run lengths.

A: Empirical cumulative probability distribution of run lengths for cargos in the clustered, rigid dispersed and free independent modes. Different total numbers of motors are shown on a common color axis.

B: Empirical cumulative probability distributions of cargos with closely matched mean numbers of motors engaged at steady state (N_{ss}). Total numbers of motors N was picked for each mode to match an N_{ss} of 2.5.

C: Percent of cargos bound as a function of time for cargos with the same total numbers of total motors N as in B, picked to match mean number of motors engaged at steady state, N_{ss}. The time before steady state is reached is filled in color below the curve for each organization mode.

S4 Fig. Means and Distributions of run lengths under force.

A: Run lengths as a function of the number of total numbers on the cargo for several values of hindering force on the cargo. Errorbars are standard error of the mean.

B: Mean run lengths as a function of external hindering load on the cargo for cargos in each of the three modes, with the total number of motors on the cargo matched at 4.

C: Distributions of run lengths of cargos under different loads. Numbers of motors are chosen to match figure 5B. Distributions are colored on a common axis corresponding to the legend in the right (free independent) panel.

S1 Video. Animation from example simulation of cargo with free independent motors. Frames in Fig 2B taken from this simulation.

S2 Video. Animation of cargo binding for cargo with rigid clustered motors.

S3 Video. Animation of cargo binding for cargo with rigid dispersed motors.

S4 Video. Animation of cargo binding for cargo with free independent motors.

S5 Video. Animation of cargo binding for cargo with free clustered motors.

S6 Video. Animation of run length for cargo with rigid clustered motors.

S7 Video. Animation of run length for cargo with rigid dispersed motors.

S8 Video. Animation of run length for cargo with free independent motors.

S1 Appendix. Mathematical Model of Cargo Transport with Motor Freedom.

S2 Appendix. On approximating a value for intracellular viscosity.

S1 Table. Fits to simulated data.

Acknowledgments

This work was supported by NIH R01 GM123068 to JA and SG, NIH T32 Training Grant EB009418-07 to Arthur Lander and Qing Nie, the UCI Center for Complex Biological Systems, the BEST IGERT program funded by the National Science Foundation DGE-1144901, NSF grant DMS 1763272 and a grant from the Simons Foundation (594598, QN).

References

1. Verhey KJ, Kaul N, Soppina V. Kinesin Assembly and Movement in Cells. Annual Review of Biophysics. 2011;40(1):267–288. doi:10.1146/annurev-biophys-042910-155310.

2. Herms A, Bosch M, Reddy BJN, Schieber NL, Fajardo A, Rupérez C, et al. AMPK activation promotes lipid droplet dispersion on detyrosinated microtubules to increase mitochondrial fatty acid oxidation. Nature Communications. 2015;6:7176. doi:10.1038/ncomms8176.

3. Maday S, Twelvetrees AE, Moughamian AJ, Holzbaur ELF. Axonal transport: cargo-specific mechanisms of motility and regulation. Neuron. 2014;84(2):292–309. doi:10.1016/j.neuron.2014.10.019.

4. Akhmanova A, Hammer JA. Linking molecular motors to membrane cargo. Current Opinion in Cell Biology. 2010;22(4):479–487. doi:10.1016/J.CEB.2010.04.008.

5. Yamada S, Wirtz D, Kuo SC. Mechanics of living cells measured by laser tracking microrheology. Biophysical Journal. 2000;78(4):1736–1747. doi:10.1016/S0006-3495(00)76725-7.

6. Wilhelm C, Gazeau F, Bacri JC. Rotational magnetic endosome microrheology: Viscoelastic architecture inside living cells. Physical Review E - Statistical Physics, Plasmas, Fluids, and Related Interdisciplinary Topics. 2003;67(6):12. doi:10.1103/PhysRevE.67.061908.

7. Saffman PG, Delbrück M. Brownian motion in biological membranes. Proceedings of the National Academy of Sciences of the United States of America. 1975;72(8):3111–3. doi:10.1073/PNAS.72.8.3111.

8. Keller S, Berghoff K, Kress H. Phagosomal transport depends strongly on phagosome size. Scientific Reports. 2017;7(1):1–15. doi:10.1038/s41598-017-17183-7.

9. Rai A, Pathak D, Thakur S, Singh S, Dubey AK, Mallik R. Dynein Clusters into Lipid Microdomains on Phagosomes to Drive Rapid Transport toward Lysosomes. Cell. 2016;164(4):722–734. doi:10.1016/j.cell.2015.12.054.

10. Erickson RP, Jia Z, Gross SP, Yu CC. How Molecular Motors Are Arranged on a Cargo Is Important for Vesicular Transport. PLoS Computational Biology. 2011;7(5):e1002032. doi:10.1371/journal.pcbi.1002032.

11. Grover R, Fischer J, Schwarz FW, Walter WJ, Schwille P, Diez S. Transport efficiency of membrane-anchored kinesin-1 motors depends on motor density and diffusivity. Proceedings of the National Academy of Sciences. 2016;113(46):E7185–E7193. doi:10.1073/pnas.1611398113.

12. Li Q, Tseng KF, King SJ, Qiu W, Xu J. A fluid membrane enhances the velocity of cargo transport by small teams of kinesin-1. The Journal of Chemical Physics. 2018;148(12):123318. doi:10.1063/1.5006806.

13. Xu J, Shu Z, King SJ, Gross SP. Tuning Multiple Motor Travel via Single Motor Velocity. Traffic. 2012;13(9):1198–1205. doi:10.1111/j.1600-0854.2012.01385.x.

14. Feng Q, Mickolajczyk KJ, Chen GY, Hancock WO. Motor Reattachment Kinetics Play a Dominant Role in Multimotor-Driven Cargo Transport. Biophysical Journal. 2018;114(2):400–409. doi:10.1016/j.bpj.2017.11.016.

15. Bergman JP, Bovyn MJ, Doval FF, Sharma A, Gudheti MV, Gross SP, et al. Cargo navigation across 3D microtubule intersections. Proceedings of the National Academy of Sciences. 2018;115(3):537–542. doi:10.1073/pnas.1707936115.

16. Chowdary PD, Kaplan L, Che DL, Cui B. Dynamic Clustering of Dyneins on Axonal Endosomes: Evidence from High-Speed Darkfield Imaging. Biophysical Journal. 2018;115(2):230–241. doi:10.1016/j.bpj.2018.05.026.

17. Milo R, Jorgensen P, Moran U, Weber G, Springer M. BioNumbersthe database of key numbers in molecular and cell biology. Nucleic Acids Research. 2010;38(SUPPL.1):750–753. doi:10.1093/nar/gkp889.

18. Shubeita GT, Tran SL, Xu J, Vershinin M, Cermelli S, Cotton SL, et al. Consequences of Motor Copy Number on the Intracellular Transport of Kinesin-1-Driven Lipid Droplets. Cell. 2008;135(6):1098–1107. doi:10.1016/j.cell.2008.10.021.

19. Klumpp S, Lipowsky R. Cooperative cargo transport by several molecular motors. Proceedings of the National Academy of Sciences. 2005;102(48):17284–9. doi:10.1073/pnas.0507363102.

20. Kunwar A, Vershinin M, Xu J, Gross SP. Stepping, Strain Gating, and an Unexpected Force-Velocity Curve for Multiple-Motor-Based Transport. Current Biology. 2008;18(16):1173–1183. doi:10.1016/j.cub.2008.07.027.

21. Lombardo AT, Nelson SR, Ali MY, Kennedy GG, Trybus KM, Walcott S, et al. Myosin Va molecular motors manoeuvre liposome cargo through suspended actin filament intersections in vitro. Nature Communications. 2017;8:15692. doi:10.1038/ncomms15692.

22. Sigurdsson JK, Atzberger PJ. Hydrodynamic coupling of particle inclusions embedded in curved lipid bilayer membranes. Soft Matter. 2016;12(32):6685–6707. doi:10.1039/c6sm00194g.

23. Andreasson JOL, Milic B, Chen GY, Guydosh NR, Hancock WO, Block SM. Examining kinesin processivity within a general gating framework. eLife. 2015;2015(4):1–44. doi:10.7554/eLife.07403.

24. Sumi T. Design principles governing chemomechanical coupling of kinesin. Scientific Reports. 2017;7(1):1163. doi:10.1038/s41598-017-01328-9.

25. Guo M, Ehrlicher AJ, Jensen MH, Renz M, Moore JR, Goldman RD, et al. Probing the stochastic, motor-driven properties of the cytoplasm using force spectrum microscopy. Cell. 2014;158(4):822–832. doi:10.1016/j.cell.2014.06.051.

26. Ahmed WW, Fodor É, Almonacid M, Bussonnier M, Verlhac MH, Gov N, et al. Active Mechanics Reveal Molecular-Scale Force Kinetics in Living Oocytes. Biophysical Journal. 2018;114(7):1667–1679. doi:10.1016/j.bpj.2018.02.009.

27. Kusumi A, Tsunoyama TA, Hirosawa KM, Kasai RS, Fujiwara TK. Tracking single molecules at work in living cells. Nature Chemical Biology. 2014;10(7):524–532. doi:10.1038/nchembio.1558.

28. Sanghavi P, D'Souza A, Rai A, Rai A, Padinhatheeri R, Mallik R. Coin Tossing Explains the Activity of Opposing Microtubule Motors on Phagosomes. Current Biology. 2018;28(9):1460–1466.e4. doi:10.1016/j.cub.2018.03.041.

29. Lüdecke A, Seidel AM, Braun M, Lansky Z, Diez S. Diffusive tail anchorage determines velocity and force produced by kinesin-14 between crosslinked microtubules. Nature Communications. 2018;9(1). doi:10.1038/s41467-018-04656-0.

30. Neefjes J, Jongsma MML, Berlin I. Stop or Go? Endosome Positioning in the Establishment of Compartment Architecture, Dynamics, and Function. Trends in Cell Biology. 2017;27(8):580–594. doi:10.1016/j.tcb.2017.03.002.

31. Pathak D, Mallik R. Lipid - Motor Interactions: Soap Opera or Symphony? Current Opinion in Cell Biology. 2017;44:79–85. doi:10.1016/j.ceb.2016.09.005.

32. Reddy BJN, Mattson M, Wynne CL, Vadpey O, Durra A, et al. Load-induced enhancement of Dynein force production by LIS1–NudE in vivo and in vitro. Nature Communications. 2016:7,1–14. doi:10.1038/ncomms12259.

33. Narayanareddy BR, Vartiainen S, Hariri N, O'Dowd DK, Gross SP. A Biophysical Analysis of Mitochondrial Movement: Differences Between Transport in Neuronal Cell Bodies Versus Processes. Traffic. 2014;15:762–771. doi:10.1111/tra.12171.

34. Allard J, Doumic M, Mogilner A, et al. Bidirectional sliding of two parallel microtubules generated by multiple identical motors J. Math. Biol. 2019;79: 571. doi:10.1007/s00285-019-01369-w.

35. Ando D, Korabel N, Huang KC, Gopinathan A. Cytoskeletal Network Morphology Regulates Intracellular Transport Dynamics. Biophysical Journal. 2015;109(8):1574–1582. doi:10.1016/j.bpj.2015.08.034.

36. Ciocanel MV, Sandstede B, Jeschonek SP, Mowry KL. Modeling Microtubule-Based Transport and Anchoring of mRNA. SIAM Journal on Applied Dynamical Systems. 2018;doi:10.1137/18M1186083.

37. Erickson RP, Gross SP, Yu CC. Filament-Filament Switching Can Be Regulated by Separation Between Filaments Together with Cargo Motor Number. PLoS ONE. 2013;8(2):e54298. doi:10.1371/journal.pone.0054298.

38. Driller-Colangelo AR, Chau KWL, Morgan JM, Derr ND. Cargo rigidity affects the sensitivity of dynein ensembles to individual motor pausing. Cytoskeleton. 2016;73(12):693–702. doi:10.1002/cm.21339.

39. Dixit R, Ross JL, Goldman YE, Holzbaur ELF. Differential regulation of dynein and kinesin motor proteins by tau. Science. 2008;319(5866):1086–9. doi:10.1126/science.1152993.

40. Vershinin M, Carter BC, Razafsky DS, King SJ, Gross SP. Multiple-motor based transport and its regulation by Tau. Proceedings of the National Academy of Sciences. 2007;104(1):87–92. doi:10.1073/pnas.0607919104.

41. Coombs D, Straube R, Ward M. Diffusion on a Sphere with Localized Traps: Mean First Passage Time, Eigenvalue Asymptotics, and Fekete Points. SIAM Journal on Applied Mathematics. 2009;70(1):302–332. doi:10.1137/080733280.

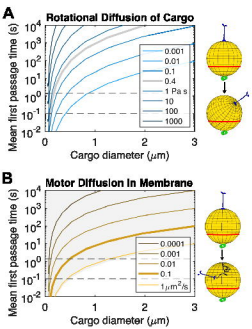
A
Rotational Diffusion of Cargo
Mean first passage time (s)
Cargo diameter (μm)
0.001
0.01
0.1
0.4
1 Pa s
10
100
1000
B
Motor Diffusion in Membrane
Mean first passage time (s)
Cargo diameter (μm)
0.0001
0.001
0.01
0.1
1 μm²/s

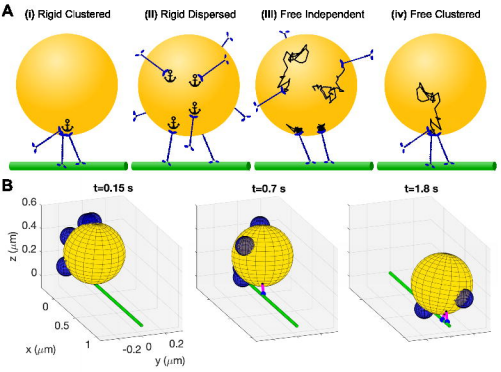
A
(i) Rigid Clustered
(II) Rigid Dispersed
(III) Free Independent
(iv) Free Clustered
B
t=0.15 s
t=0.7 s
t=1.8 s
z (μm)
0.6
0.4
0.2
0
x (μm)
0
0.5
1
y (μm)
-0.2
0
0.2

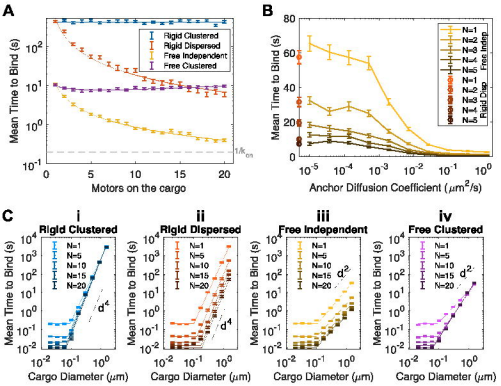
A
Mean Time to Bind (s)
Motors on the cargo
Rigid Clustered
Rigid Dispersed
Free Independent
Free Clustered
1/k_on
B
Mean Time to Bind (s)
Anchor Diffusion Coefficient (μm²/s)
N=1
N=2
N=3
N=4
N=5
Free Indep.
Rigid Disp.
C
i
Rigid Clustered
ii
Rigid Dispersed
iii
Free Independent
iv
Free Clustered
Mean Time to Bind (s)
Cargo Diameter (μm)
N=1
N=5
N=10
N=15
N=20
d⁴
d²

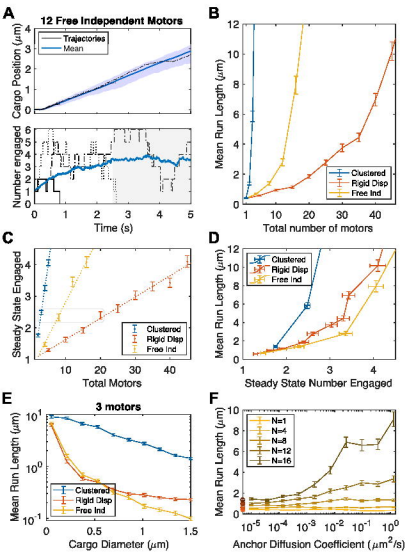
A
12 Free Independent Motors
Trajectories
Mean
Cargo Position (μm)
Number engaged
Time (s)
B
Mean Run Length (μm)
Total number of motors
Clustered
Rigid Disp
Free Ind
C
Steady State Engaged
Total Motors
Clustered
Rigid Disp
Free Ind
D
Mean Run Length (μm)
Steady State Number Engaged
Clustered
Rigid Disp
Free Ind
E
3 motors
Mean Run Length (μm)
Cargo Diameter (μm)
Clustered
Rigid Disp
Free Ind
F
Mean Run Length (μm)
Anchor Diffusion Coefficient (μm²/s)
N=1
N=4
N=8
N=12
N=16

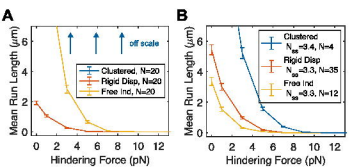
A
Mean Run Length (μm)
Hindering Force (pN)
off scale
Clustered, N=20
Rigid Disp, N=20
Free Ind, N=20
B
Mean Run Length (μm)
Hindering Force (pN)
Clustered
N_ss=3.4, N=4
Rigid Disp
N_ss=3.3, N=35
Free Ind
N_ss=3.3, N=12

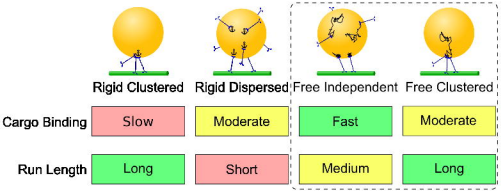
Rigid Clustered
Rigid Dispersed
Free Independent
Free Clustered
Cargo Binding
Slow
Moderate
Fast
Moderate
Run Length
Long
Short
Medium
Long

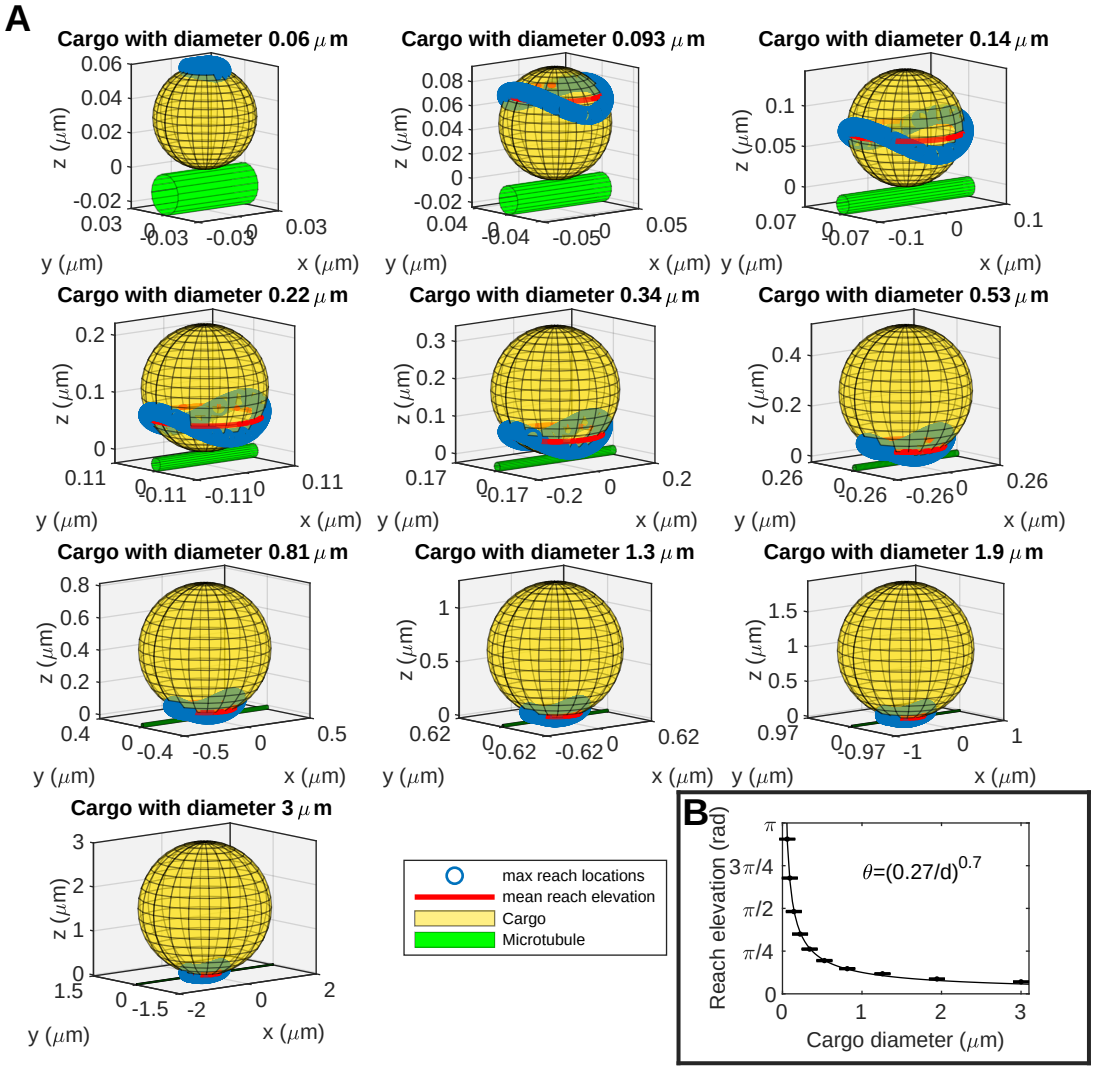
A
Cargo with diameter 0.06 μm
Cargo with diameter 0.093 μm
Cargo with diameter 0.14 μm
Cargo with diameter 0.22 μm
Cargo with diameter 0.34 μm
Cargo with diameter 0.53 μm
Cargo with diameter 0.81 μm
Cargo with diameter 1.3 μm
Cargo with diameter 1.9 μm
Cargo with diameter 3 μm
z (μm)
y (μm)
x (μm)
max reach locations
mean reach elevation
Cargo
Microtubule
B
Reach elevation (rad)
Cargo diameter (μm)
θ=(0.27/d)^0.7
π
3π/4
π/2
π/4
0
1
2
3

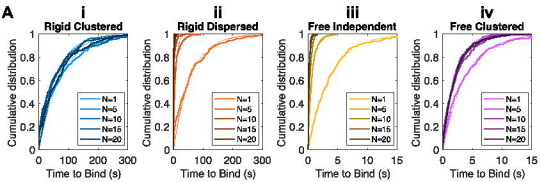
A
i
Rigid Clustered
ii
Rigid Dispersed
iii
Free Independent
iv
Free Clustered
Cumulative distribution
Time to Bind (s)
N=1
N=5
N=10
N=15
N=20

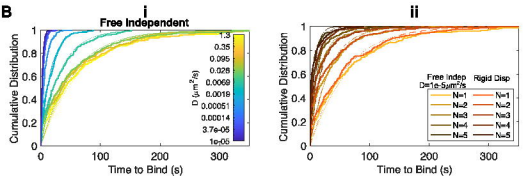
B
i
Free Independent
ii
Cumulative Distribution
Time to Bind (s)
D (μm²/s)
1.3
0.35
0.095
0.026
0.0069
0.0018
0.00051
0.00014
3.7e-05
1e-05
Free Indep
D=1e-5μm²/s
Rigid Disp
N=1
N=2
N=3
N=4
N=5

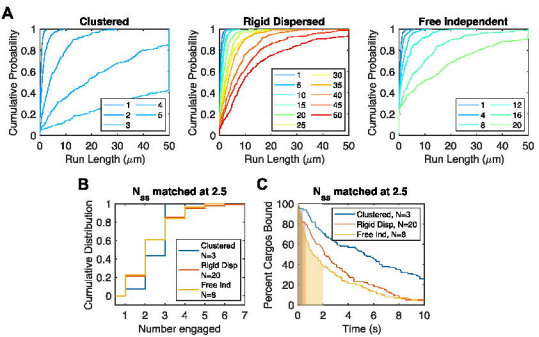
A
Clustered
Rigid Dispersed
Free Independent
Cumulative Probability
Run Length (μm)
1
2
3
4
5
1
5
10
15
20
25
30
35
40
45
50
1
4
8
12
16
20
B
N_ss matched at 2.5
Cumulative Distribution
Number engaged
Clustered N=3
Rigid Disp N=20
Free Ind N=8
C
N_ss matched at 2.5
Percent Cargos Bound
Time (s)
Clustered, N=3
Rigid Disp, N=20
Free Ind, N=8

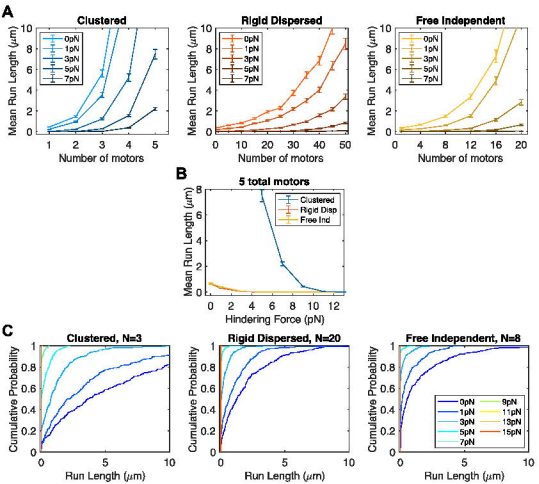
A
Clustered
Rigid Dispersed
Free Independent
Mean Run Length (μm)
Number of motors
0pN
1pN
3pN
5pN
7pN
B
5 total motors
Clustered
Rigid Disp
Free Ind
Hindering Force (pN)
C
Clustered, N=3
Rigid Dispersed, N=20
Free Independent, N=8
Cumulative Probability
Run Length (μm)
0pN
1pN
3pN
5pN
7pN
9pN
11pN
13pN
15pN